

An intronic deletion in the *PROM1* gene leads to autosomal recessive cone-rod dystrophy

Osnat Eidinger,¹ Rina Leibur,² Hadas Newman,^{3,4} Leah Rizel,¹ Ido Perlman,^{1,3} Tamar Ben-Yosef¹

¹Ruth and Bruce Rappaport Faculty of Medicine, Technion-Israel Institute of Technology, Haifa, Israel; ²Alberto Moscona Department of Ophthalmology, Rambam Health Care Center, Haifa, Israel; ³Department of Ophthalmology, Tel-Aviv Souraski Medical Center, Tel-Aviv, Israel; ⁴Sackler Faculty of Medicine, Tel Aviv University, Tel Aviv, Israel

Purpose: To investigate the genetic basis for autosomal recessive cone-rod dystrophy (CRD) in a consanguineous Israeli Jewish family.

Methods: Patients underwent a detailed ophthalmic evaluation, including eye examination, visual field testing, optical coherence tomography (OCT), and electrophysiological tests, electroretinography (ERG) and visual evoked potential (VEP). Genome-wide homozygosity mapping using a single nucleotide polymorphism (SNP) array was performed to identify homozygous regions shared among two of the affected individuals. Mutation screening of the underlying gene was performed with direct sequencing. In silico and in vitro analyses were used to predict the effect of the identified mutation on splicing.

Results: The affected family members are three siblings who have various degrees of progressive visual deterioration, glare, color vision abnormalities, and night vision difficulties. Visual field tests revealed central scotomas of different extension. Cone and rod ERG responses were reduced, with cones more severely affected. Homozygosity mapping revealed several homozygous intervals shared among two of the affected individuals. One included the *PROM1* gene. Sequence analysis of the 26 coding exons of *PROM1* in one affected individual revealed no mutations in the coding sequence or in intronic splice sites. However, in intron 21, proximate to the intron-exon junction, we observed a homozygous 10 bp deletion between positions -26 and -17 (c.2281-26_-17del). The deletion was linked to a known SNP, c.2281-6C>G. The deletion cosegregated with the disease in the family, and was not detected in public databases or in 101 ethnically-matched control individuals. In silico analysis predicted that this deletion would lead to altered intron 21 splicing. Bioinformatic analysis predicted that a recognition site for the SRSF2 splicing factor is located within the deleted sequence. The in vitro splicing assay demonstrated that c.2281-26_-17del leads to complete exon 22 skipping.

Conclusions: A novel and unique intronic mutation of *PROM1*, underlying autosomal recessive CRD in a consanguineous Israeli family, was found. This report expands the spectrum of pathogenic mutations of *PROM1* and further demonstrates the importance of intronic mutations.

Inherited retinal dystrophies (IRDs) are a clinically and genetically heterogeneous group of diseases that cause visual loss due to the progressive loss of rod and/or cone photoreceptor cells in the retina. One form of IRD is cone-rod dystrophy (CRD), in which cone involvement initially exceeds that of rods, and therefore, the predominant symptoms are reduced visual acuity, photophobia, defective color vision, and central scotoma. Only later, as the disease progresses, peripheral vision and night blindness follow. Additional ophthalmologic findings include pigment deposits visible on fundus examination, predominantly localized to the macular region. The prevalence of CRD is approximately 1/40,000 [1,2].

CRD is a heterogeneous disorder. In most patients, the disease is limited to the eye (non-syndromic), with no extra-ocular manifestations. Non-syndromic CRD can be inherited as autosomal recessive, autosomal dominant, or X-linked. More than 20 genes have been implicated in non-syndromic CRD (RetNet- Retinal Information Network). One is *PROM1* (GenBank accession number [NM_006017](#); OMIM [604365](#)).

PROM1 encodes prominin 1, a five-transmembrane domain glycoprotein, which was originally identified as CD133/AC133, a surface antigen of human hematopoietic stem and progenitor cells [3,4]. *PROM1* localizes to plasma membrane evaginations of neuroepithelial stem cells and several other epithelial cell types [5]. In the retina, *PROM1* is concentrated in the base of photoreceptor outer segments, where the protein is involved in photoreceptor disk morphogenesis [6]. Mutations of *PROM1* have been associated with a variety of retinal phenotypes, including autosomal recessive retinitis pigmentosa with macular degeneration (RP41), autosomal dominant Stargardt-like macular dystrophy (STGD4),

Correspondence to: Tamar Ben-Yosef, Department of Genetics, Rappaport Faculty of Medicine, Technion, P.O. Box 9649, Bat Galim, Haifa 31096, Israel; Phone: 972-4-829-5228; FAX: 972-4-829-5225; email: benyosef@tx.technion.ac.il

TABLE 1. *PROM1* MUTATIONS IDENTIFIED IN PATIENTS WITH INHERITED RETINAL DYSTROPHIES,

Exon / Intron	Base Change	Amino Acid Substitution	Phenotype	Reference
Recessive Mutations				
Exon 4	c.442A>T	p.K148X	arRP	[18]
Exon 5	c.622delA	p.T208Lfs22X	arRP	[19]
Exon 6	c.642T>A	p.Y214X	arRP	[20]
Exon 7	c.730C>T	p.R244X	arCRD	[21]
Exon 8	c.869delG	p.S290LfsX	arRP with macular degeneration	[22]
Intron 10	c.1142-1G>A		arCRD	[7]
Exon 11	c.1157T>A	p.L386X	arCRD	[23]
Exon 11	c.1209-1229del	p.Q403-S410del;insH	arRP	[20]
Exon 12	c.1349insT	p.Y452Ffs38X	arCRD	[9]
Exon 12	c.1355_1356insT	p.Y453Lfs11X	arRP	[19]
Intron 12	c.1454+2T>C		arCRD	[24]
Intron 13	c.1579-1G>C		arCRD	[24]
Exon 15	c.1697dupA	p.N566KfsX	arCRD	[25]
Exon 15	c.1726C>T	p.Q576X	arRP with macular degeneration	[26]
Exon 16	c.1841delG	p.G614Efs12X	arRP with macular degeneration	[8]
Intron 17	c.1983+1G>T		arCRD	[21]
Intron 17	c.1984-1G>T		arCRD	[24]
Intron 18	c.2077-521A>G		arCRD	[17]
Intron 21	c.2281-26_-17del	p.I761-L791del	arCRD	Current study
Exon 23	c.2383T>C	p.W795R	arCRD	[24]
Dominant Mutations				
Exon 1	c.7dup	p.L3Pfs28X	adCRD	[24]
Exon 10	c.1117C>T	p.R373C	ad Stargardt-like MD, ad bull's-eye MD, adCRD	[6]

ar, autosomal recessive; ad, autosomal dominant; RP, retinitis pigmentosa; CRD, cone-rod dystrophy; MD, macular dystrophy

autosomal dominant bull's-eye macular dystrophy (MCDR2), autosomal dominant CRD (CORD12), and autosomal recessive CRD [6-9].

To date, 21 distinct pathogenic mutations of *PROM1* have been reported; 19 of them are associated with an autosomal recessive mode of inheritance (Table 1 and Figure 1A). Here, we report a novel and unique intronic mutation of *PROM1*, which affects splicing.

METHODS

Subjects and clinical evaluation: The study protocol was in accordance with the tenets of the Declaration of Helsinki and the ARVO (Association for Research in Vision and Ophthalmology) statement on human subjects. Written informed consent was obtained from the participants or their parents. The research was approved by the local institutional review

board at Rambam Health Care Center and by the National Helsinki Committee for Genetic Research in Humans. Anonymous ethnically-matched DNA control samples were obtained from the National Laboratory for the Genetics of the Israeli Population at Tel Aviv University.

The ophthalmic evaluation of the affected individuals included best-corrected visual acuity (BCVA), color fundus photos, spectral domain-optical coherence tomography (SD-OCT) of the macula, visual fields (VFs) Swedish Interactive Thresholding Algorithm (SITA) Fast 24-2, pattern and flash visual evoked potentials (VEPs), and full-field and multifocal electroretinography (ff-ERG and mf-ERG, respectively). ff-ERG recordings were performed at MARAH Ltd in Rambam Health Care Center, Haifa, Israel, using the UTAS BigShot electrophysiological system (LKC Technologies, Gaithersburg, MD), with bipolar Burian-Allen corneal electrodes (Hansen Ophthalmic Development, Coralville, IA)

with a slightly modified protocol compared to International Society for Clinical Electrophysiology of Vision (ISCEV) standards [10]. mf-ERG recordings were performed at the Vision Electrophysiology Unit, Department of Ophthalmology, Tel Aviv Sourasky Medical Center, using the Espion E³ system (Diagnosis LLC, Lowell, MA). Different hexagon arrays were used with luminance setting of 1,000 cd/m². Corneal bipolar contact lenses (Burian-Allen Electrodes) were used in patients II-3 and II-4, while a Dawson, Trick, and Litzkow (DTL) electrode was used in patient II-1.

DNA analysis: Venous blood samples were obtained using K3 EDTA Vacuette tubes (Greiner Bio-One, Kremsmunster, Austria), and genomic DNA was extracted using a high salt solution according to a standard protocol [11]. Genome-wide homozygosity mapping was performed using

the HumanCytoSNP-12v2.1 BeadChip (220 K; Illumina, Inc., San Diego, CA). Homozygous regions were calculated using *HomozygosityMapper* [12] with a lower threshold of 1 Mb. For mutation analysis specific primers were used to PCR-amplify the 26 coding exons of *PROM1*, including intron-exon boundaries. Primer sequences were as previously described [9]. PCR was performed in a 25 µl reaction volume in the presence of 5X ReadyMix (LAROVA GmbH, Teltow, Germany) and 10 pmol of each forward and reverse primers. Annealing temperature was 60 °C. Mutation screening was performed with direct sequencing with the BigDye Terminator Cycle Sequencing kit on an ABI 3130xl Genetic Analyzer (PE Applied Biosystems, Foster City, CA).

In vitro splicing assay: To create wild-type (wt) and mutant minigene constructs, DNA fragments harboring *PROM1*

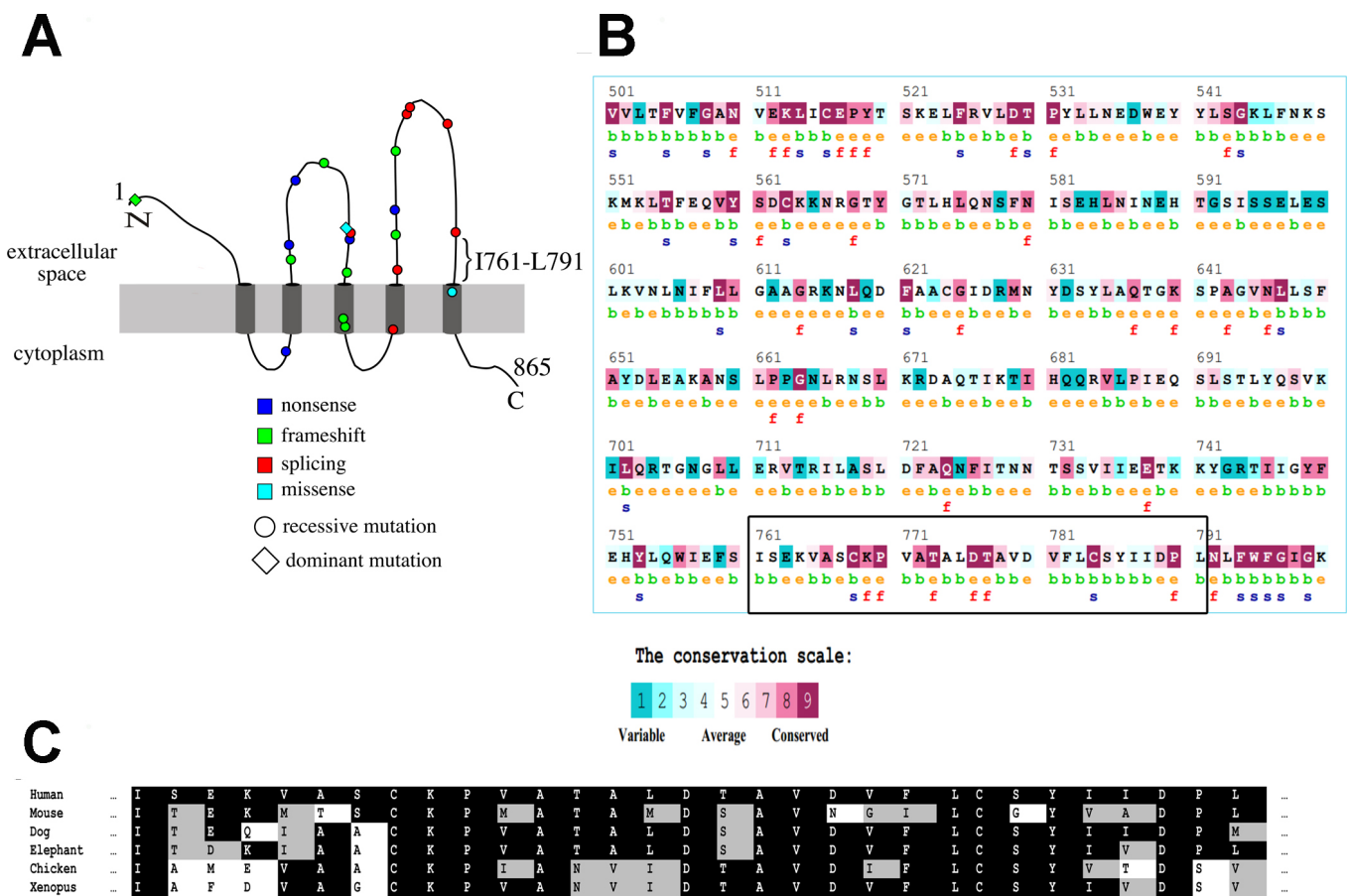


Figure 1. The *PROM1* protein. **A:** Shown is a schematic representation of the *PROM1* protein and the location of pathogenic mutations reported to date. For frameshift and splicing mutations, the mark indicates the location of the first affected amino acid. The location of amino acids I761–L791, encoded by exon 22, is indicated. The illustration is based on [16]. **B:** Evolutionary conservation of the *PROM1* second extracellular loop. The analysis was performed with the ConSurf Server based on 108 *PROM1* orthologs. Amino acids 761–791, included in the deletion, are marked by a box. e, an exposed residue; b, a buried residue; f, a predicted functional residue (highly conserved and exposed); s, a predicted structural residue (highly conserved and buried). **C:** Multiple sequence alignment of *PROM1* amino acids encoded by exon 22 in various organisms. Conserved amino acids are indicated by a black background. Similar amino acids are indicated by a gray background.

exons 21, 22, and 23, each flanked by 68–232 bp of intronic sequences, were PCR amplified from the genomic DNA of patients and controls. The fragments were inserted in tandem into the pCMV-Script mammalian expression vector (Stratagene, La Jolla, CA). Constructs were transfected into COS-7 cells, using the jetPEI transfection reagent (Polyplus transfection, Illkirch, France). Cells were cultured in DMEM culture medium supplemented with 10% fetal bovine serum (Biologic Industries, Beit Ha'emek, Israel) and maintained at 37 °C and 5% CO₂. Twenty-four hours following transfection, total RNA was extracted from cells with TRI reagent (Sigma-Aldrich, St. Louis, MO). Reverse transcription was performed with 1 µg of total RNA in a 20 µl reaction volume using 200U of M-MLV Reverse Transcriptase and 100 ng of random primers (Stratagene, La Jolla, CA). Two µl of cDNA were subjected to PCR amplification with primers located in exons 21 and 23. COS-7 cells used for this experiment were authenticated by genotyping four short tandem repeat (STR) markers (D17S1304, D5S1467, D4S2408, D19S245). Genotyping was performed by PCR amplification of each STR and direct sequencing, as described by Almeida et al. [13]. Results (in terms of repeat number for each STR) were compatible with those described for COS-7 cells [13] (Appendix 1).

RESULTS

Clinical findings: Family TB126 is a Jewish family of Kurdish Iraqi descent. The parents are remotely related, and three of their four offspring were diagnosed with CRD (Figure 2A).

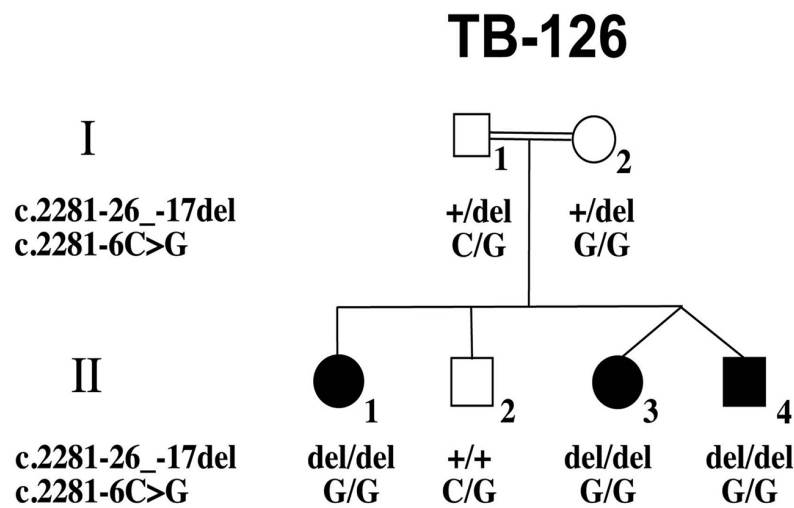
The family members underwent extensive electrophysiological and clinical testing to define the type of retinal disorder (Figures 3 and Figure 4 and Table 2). The eldest daughter (individual II-1) first complained of visual deterioration at the age of 7 years and was diagnosed with CRD at the age of 9 years. At this age, her ff-ERG test showed sub-normal photopic retinal function and normal scotopic retinal function. Over the next few years, she had symmetric progressive visual deterioration accompanied by progressive central visual field loss and reduction in night vision. At the age of 17 years, she complained of glare, deficient color vision, and night vision abnormalities. Her central VF was severely compromised presenting small paracentral islands of residual vision. Funduscopy of both eyes revealed macular confluent sheen with central pigmentary dispersion and paracentral pigmentary deposits (bull's-eye maculopathy), associated with peripheral depigmented areas (Figure 3A,B). On OCT imaging, thinning of the inner retina and absence of the photoreceptor cell layer were observed (Figure 3D,E). ff-ERG responses were indicative of severely reduced cone function and rod function of the peripheral retina under photopic and

scotopic conditions (Figure 4, first row and Table 2). The VEP recordings in response to pattern reversal visual stimuli were severely compromised even in response to the largest check size (144 min of arc), indicating significantly reduced visual acuity and abnormal macular function of both eyes. The flash VEP responses consisted of waves of normal amplitude appearing at normal implicit time, indicating normal conductance in the optic nerves from each eye to the visual cortex. The Arden ratio of the electro-oculogram (EOG) results was within the normal range in both eyes, indicating normal function of the RPE layer (Table 2). mf-ERG recorded at the age of 19 years did not demonstrate measurable responses.

Individuals II-3 and II-4 are dizygotic twins (Figure 2A). Individual II-3 complained of glare and night vision abnormalities since the age of 6 years. At the age of 8 years, she had reduced visual acuity. VF testing showed bilateral paracentral scotomas. Funduscopy revealed tiny pigmentary dispersion at the macular area with depigmented flecks at the mid-periphery. Macular OCT revealed thinning of the inner retinal layers and irregularity of the photoreceptor cell layer (Figure 3G,H). ff-ERG indicated severely reduced photopic and scotopic retinal function (Figure 4, second row and Table 2). The bright flash ERG response was better than that of her older sister (II-1; Table 2). The pattern VEP responses included P₁₀₀ waves of normal amplitude and delayed latency, indicating reduced visual acuity and subnormal macular function. Flash VEP recordings in response to bright light stimuli consisted of waves of normal amplitude and normal implicit time, indicating normal transmission of the visual pathways (Table 2). mf-ERG recordings were performed using a 103-hexagon array, which stimulated the central 80° of the retina. Foveal response amplitudes were severely reduced, while peripheral responses (starting from 10° radius from fixation point) were better preserved but demonstrated amplitude reduction and delayed implicit times (Figure 3I).

Individual II-4 started complaining of subnormal vision, defective color saturation, and photosensitivity at the age of 9 years. VF testing showed bilateral extensive central scotomas. His fundus appearance revealed yellowish central spots (Figure 3C). Macular OCT revealed thinning of the inner retinal layers, irregularity of the photoreceptor cell layer, and thinning of the RPE (Figure 3F). Flash ERG on a short protocol indicated severely reduced photopic retinal function and moderately reduced scotopic retinal function (Table 2). The pattern VEP recordings in response to the pattern reversal stimuli of different check sizes included P₁₀₀ waves of slightly reduced amplitude appearing at prolonged implicit time, indicating reduced visual acuity and subnormal macular function. The flash VEP recordings in response to bright

A



B

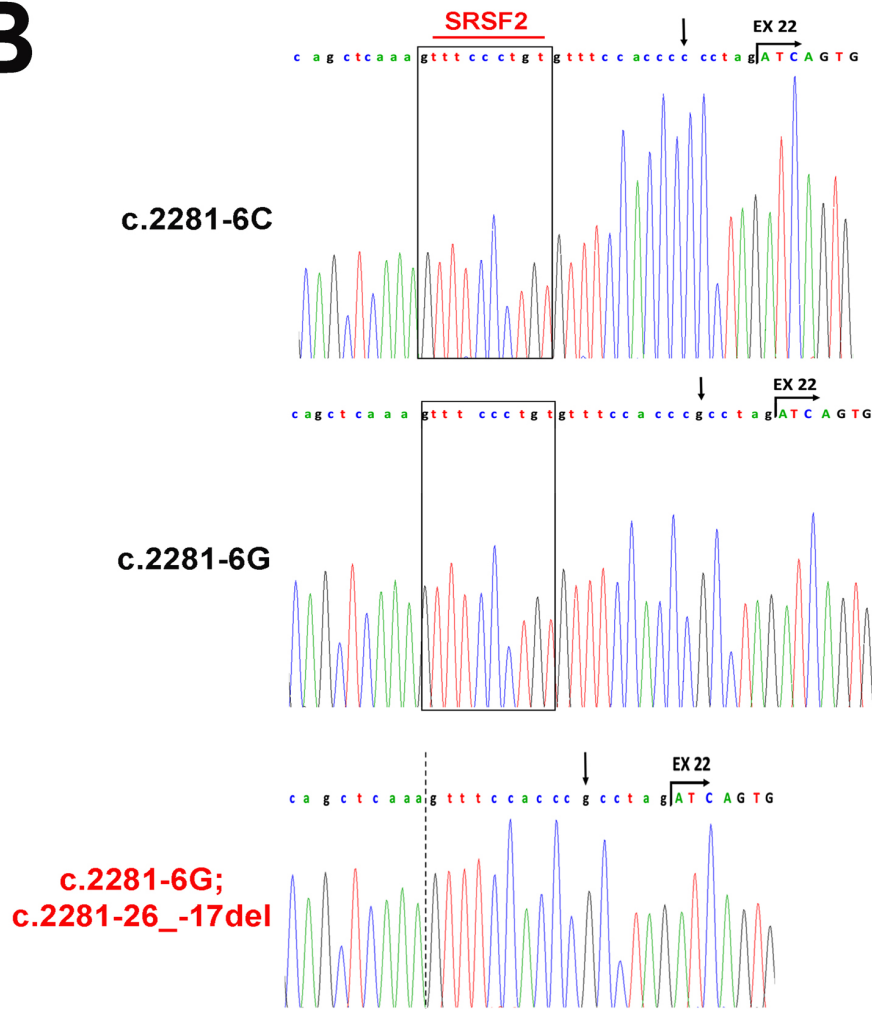


Figure 2. Pedigree and mutation analysis. **A:** Shown is an Israeli Jewish family in which the c.2281–26_-17del mutation is segregated. Filled symbols represent affected individuals, whereas clear symbols represent unaffected individuals. A double line represents a consanguineous marriage. Genotypes of family members are indicated below them. Del, deletion; +, no deletion. **B:** Shown are nucleotide sequence traces of the border between *PROM1* intron 21 and exon 22, in an individual homozygous for the c.2281–6C allele (top), an individual homozygous for the c.2281–6G allele (middle), and an individual homozygous for the c.2281–6G allele and the c.2281–26_-17 deletion (bottom). The position of the c.2281–6C>G allele is indicated by an arrow. The deletion breakpoint is indicated by a dashed line in the bottom image, while the deleted bases are indicated by a box in the corresponding wild-type (wt) sequences (top and middle). The intron–exon border is marked by a curved arrow. The location of a putative binding site for SRSF2 is marked by a red line.

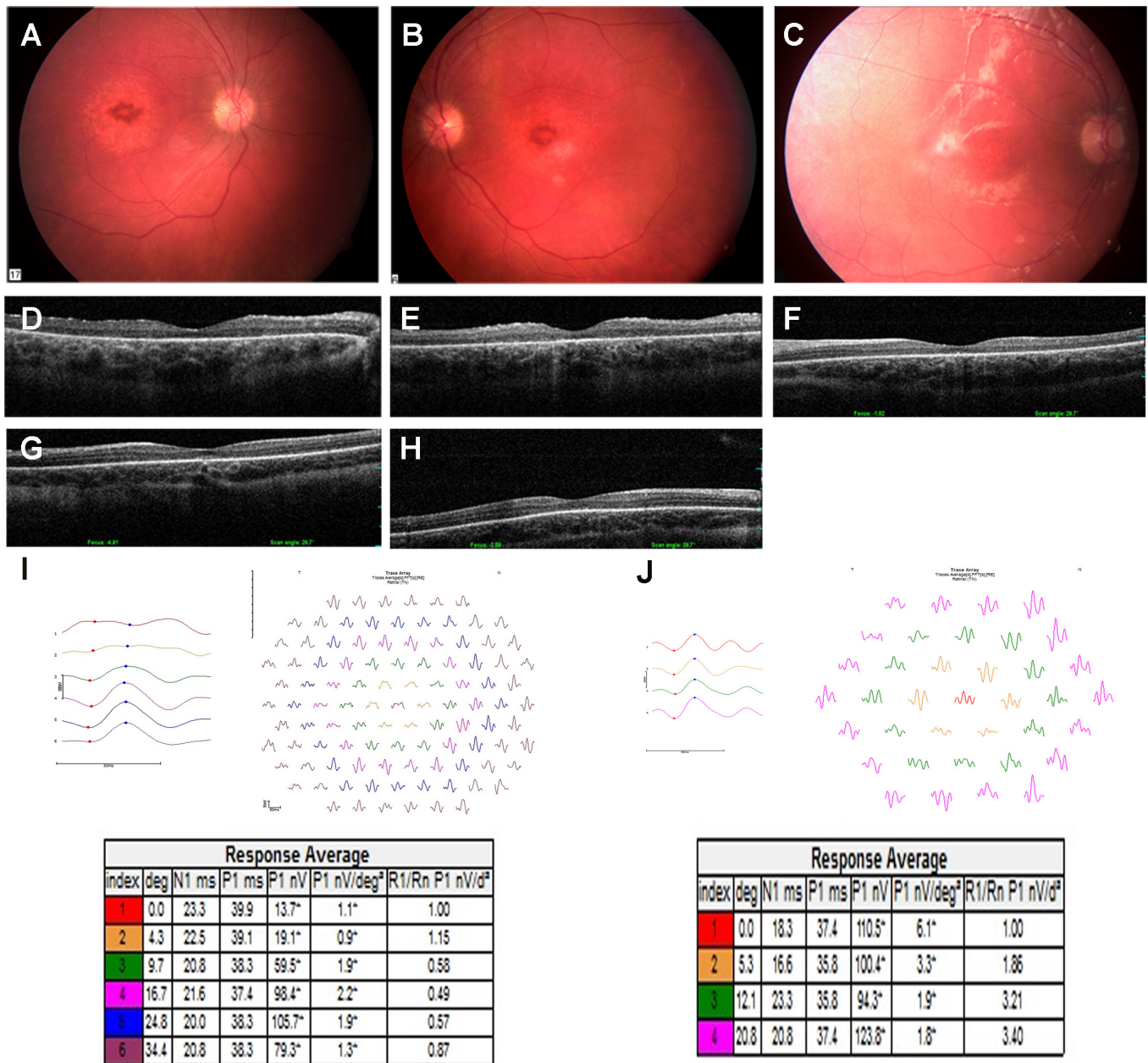


Figure 3. Clinical imaging and mf-ERG testing of affected individuals from family TB126. **A, B:** Fundus photographs of the right and left eyes of individual II-1, respectively, showing severe atrophic changes in the retina with bull’s-eye maculopathy. **C:** Fundus photograph of the right eye of individual II-4, showing diffuse pigmentary granularity and depigmented areas. **D, E:** Spectral domain-optical coherence tomography (SD-OCT) of the right and left eyes of individual II-1, respectively, showing thinning of the retina, with loss of the photoreceptor layer and atrophy of the RPE. **F:** SD-OCT of the right eye of individual II-4, showing thinning of the inner retinal layers, irregularity of the photoreceptor cell layer, and thinning of the RPE. **G, H:** SD-OCT of the right and left eyes of individual II-3, respectively, showing thinning of the inner retinal layers and irregularity of the photoreceptor cell layer. **I:** Multifocal electroretinography (mf-ERG) recordings of individual II-3, using bipolar Burian-Allen corneal electrodes. The stimulus consisted of 103-hexagon array, which stimulated the central 80° of the retina, and has maximum illumination of 1,000 cd/m². Foveal response amplitudes are severely reduced, while peripheral responses (starting from 10° radius from fixation point) are better preserved but demonstrate severe amplitude reduction and delay in implicit times. **J:** mf-ERG recordings in individual II-4, using a Dawson, Trick, and Litzkow (DTL) electrode. The stimulus consisted of a 37-hexagon array with a maximum intensity of 1,000 cd/m², which stimulated the central 48° of the retina. Response amplitudes are severely reduced in all retinal regions. Central response amplitudes are more severely reduced, with relative preservation of response amplitudes in the peripheral nasal retina (12° radius from the fixation point).

light stimuli were normal, reflecting normal conductance of the visual pathways (Table 2). mf-ERG recordings were performed using a 37-hexagon array, which stimulated the central 48° of the retina. Response amplitudes were severely reduced in all points tested. Central response amplitudes were more severely reduced, with relative preservation of response amplitudes in the peripheral nasal retina (12° radius from fixation point; Figure 3J).

Genetic analysis: Family TB126 is consanguineous, and CRD segregates in an autosomal recessive mode. We therefore performed genome-wide homozygosity mapping using the HumanCytoSNP-12v2.1 BeadChip (220 K) on

two affected individuals (Figure 2A, individuals II-1 and II-3). Several homozygous intervals ranging from 2.5 to 16.7 Mb were shared among the affected individuals. The only IRD causative gene included in a homozygous interval was *PROM1* (Table 3). Sequence analysis of the 26 coding exons of *PROM1* in one affected individual revealed no mutations in the coding sequence or in intronic splice sites. However, in intron 21 and proximate to the intron–exon junction, we observed a combination of a single base transversion at position –6 (g.4:15985984 C>G; c.2281–6C>G) and a 10-base deletion between positions –26 and –17 (g.4:15985995–15986004del; c.2281–26_–17del), both in a homozygous state

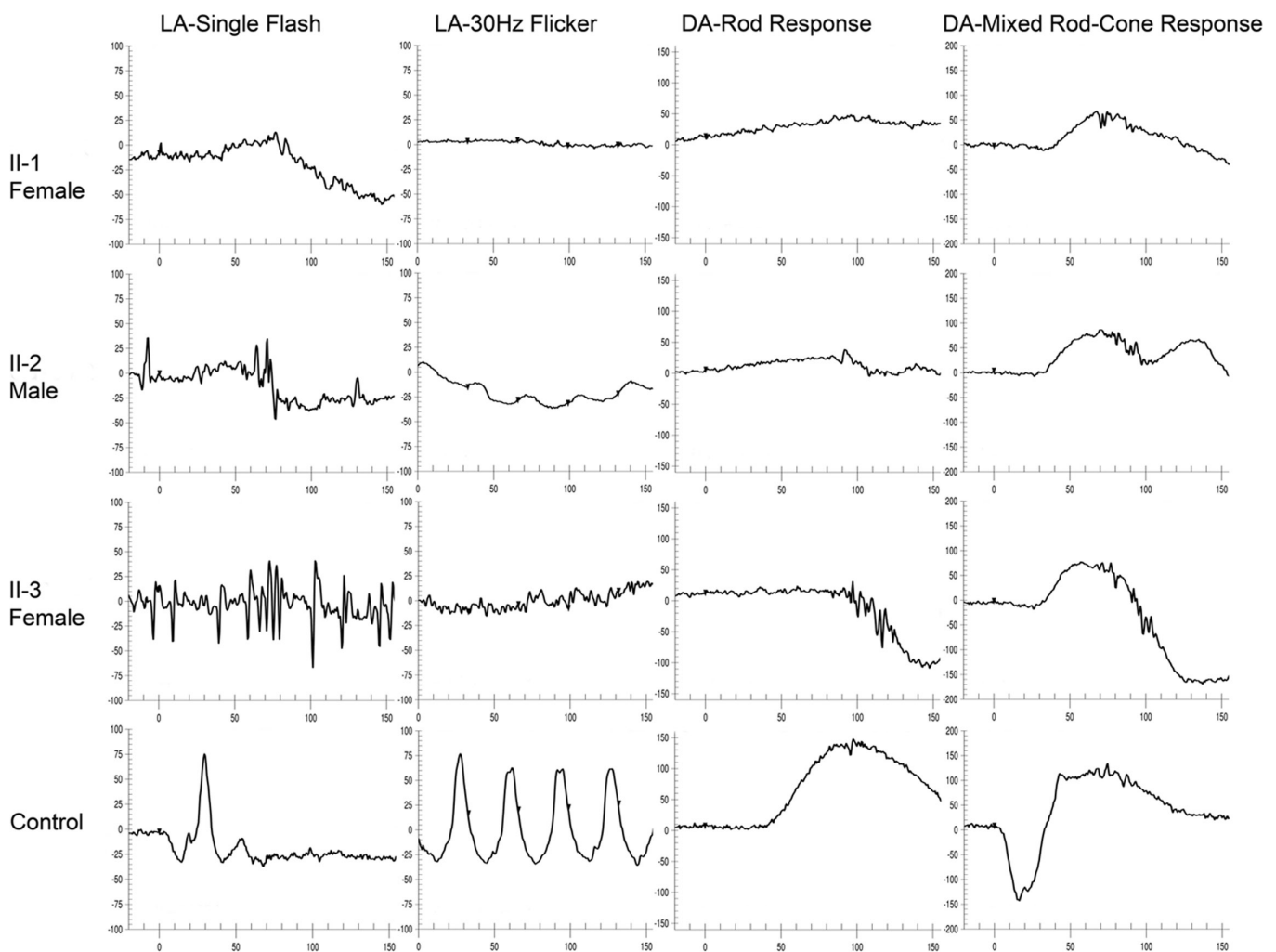


Figure 4. ff-ERG responses were recorded using Burian-Allen bipolar corneal electrodes from all three affected individuals using a slightly modified procedure compared to the International Society for Clinical Electrophysiology of Vision (ISCEV) standard [10]. Cone single response (2.5 cd-s/m²) and 30 Hz flicker (2.5 cd-s/m²) were applied during background illumination (30 cd/m²). After 20 min (shorter for individual II-3), rod response was recorded using dim blue stimulus, and mixed rod-cone was elicited with a white (2.5 cd-s/m²) stimulus. The full field electroretinography (ff-ERG) responses of the affected individuals (II-1, II-3, II-4) indicate severe deterioration of cone function and rod function with residual mixed rod-cone responses (rows 1, 2, 3, respectively) in comparison to an individual with normal retina function (fourth row). The y-axis of each response indicates amplitude (µV), and the x-axis indicates time (ms) after the stimulus onset (time=0).

TABLE 2. CLINICAL CHARACTERISTICS OF AFFECTED INDIVIDUALS FROM FAMILY TB126.

Patient No. Sex	Age (y)	Best-Corrected Visual Acuity	ffERG ^{a,b}		Flicker (30Hz) ^d Amp Latency (µV; mS)	DA Rod response (µV) ^e	Mixed Rod-Cone (Moderate stimulus) (µV) ^f	Mixed Rod-Cone (Bright stimulus) (µV) ^h	Pattern VEP P100	Flash VEP	EOG Arden ratio ⁱ	Color vision ^j	Visual Field
			LA Single flash ^c Amp Latency (µV; mS)	DA Rod response (µV) ^e									
II-1 F	17	OD 3/60 OS 6/60	12; 57	0	15	a 11 b 77	a 16 b 84	No typical responses were recorded (BE)	Typical waves of normal latency (BE)	OD 1.92 OS 1.86	Ish: BE 1 st panel not seen D-15: with BE no typical axis was observed (BE)	Large central scotomas	
II-3 F	8	OD 6/12 OS 6/12	0	0	0	a 10 b 90	a 17 b 76	Normal amplitudes and delayed latency (BE)	Typical waves of normal latency (BE)	ND	ND	Paracentral scotomas (BE)	
II-4 M	9	OD 6/12 OS 6/20	14; 42	11; 41	0	a 7 b 84	a 27 b 89	Slightly reduced amplitudes and prolonged latency (BE)	Typical waves of normal latency (BE)	ND	ND	Extensive central scotomas (BE)	

^a Full-Field Electroretinogram; LA: light adaptation (cone ERG); DA: dark adaptation (rod and cone ERG) ^b Data are presented for the right eye only. Left eye was not tested. ^c LA: single flash (2.5 cd-s/m²); Normal amplitude (Amp): minimum 70 µV; Normal latency: maximum 32 ms ^d LA: flicker (30 Hz, 2.5 cd-s/m²); Normal amplitude (Amp): minimum 50 µV; Normal latency: maximum 30 ms ^e DA: Rod response: Normal amplitude minimum 70 µV ^f DA: Mixed rod cone moderate stimulus (2.5 cd-s/m²); Normal a-wave: minimum 80 µV; Normal b-wave minimum 150 µV ^h DA: Mixed rod cone bright stimulus (25 cd-s/m²); Normal a-wave 180–280 µV; Normal b-wave 200–360 µV ⁱ EOG: Electrooculogram; Normal Arden ratio >2.0 ^j Color Vision: Ish=Ishihara Pseudoisochromatic plates color test; D-15 - Farnsworth Dichotomous Test Panel D-15 F: Female; M: Male; OD: right eye; OS: left eye; ND: Not Determined

TABLE 3. HOMOZYGOSITY MAPPING RESULTS IN FAMILY TBI26.

Chromosome	Interval of Homozygosity (Mb)	Interval Size (Mb)	IRD-related Genes
16	31.8–48.5	16.7	
11	49.3–55.2	5.9	
18	15.1–19.4	4.3	
4	14.8–17.3	2.5	<i>PROM1</i>

(Figure 2B; cDNA position refers to GenBank accession number NM_006017; genomic positions refer to reference genome GRCh37/hg19). c.2281–6C>G is a known single nucleotide polymorphism (SNP; dbSNP ID: rs3815344). In a panel of 101 ethnically-matched healthy control individuals, we found 11 homozygotes and 48 heterozygotes for the G allele. In contrast, c.2281–26₋₁₇del was not detected in the 1000 genomes database, in the ExAC Browser, or in the same panel of 101 ethnically-matched controls. In addition, c.2281–26₋₁₇del cosegregated with the disease in the family, while c.2281–6C>G appeared in a homozygous state in the unaffected mother (Figure 2A).

In silico analysis of c.2281–26₋₁₇del: Due to the proximity of c.2281–26₋₁₇del to the intron–exon junction, we hypothesized that the deletion might affect splicing. To test this hypothesis, we first performed in silico analysis of the sequence using two web-based tools: Splice Site Prediction by Neural Network and SplicePort. Both predicted that the deletion leads to elimination of the intron 21 acceptor site. According to SplicePort, the deletion would lead to elimination of the intron 21 acceptor site with either a C or a G at the –6 position. According to Splice Site Prediction by Neural Network, a combination of the deletion with a C at position –6 would lower the score of the acceptor site, while a combination of the deletion with a G at position –6 (as it appears in our patients) would completely eliminate it (Table 4).

We then analyzed the sequence for the existence of splicing enhancer sequences, with the web-based tool Human Splicing Finder (HSF). The analysis indicated that a recognition site for serine/arginine-rich splicing factor 2 (SRSF2; previously known as SC35) [14,15] is located between positions –25 and –18 of intron 21. This site (TTTCCCTG) is included in the c.2281–26₋₁₇ deletion (Figure 2B).

In vitro splicing assay: RT–PCR analysis of *PROM1* expression in white blood cells and skin fibroblasts was negative. Therefore, we could not evaluate the effect of the deletion on splicing in patient-derived RNA. Alternatively, we used an in vitro splicing assay approach. For this purpose, we created a set of minigene constructs that harbor *PROM1* exons 21 to 23, flanked by 68–232 bp of intronic sequences, downstream of a cytomegalovirus (CMV) promoter (Figure 5A). Constructs were transfected into COS-7 cells, followed by RNA extraction and RT–PCR analysis with primers located in exons 21 and 23. To analyze the results, we sequenced the splicing products derived from each construct. cDNA derived from the construct harboring the c.2281–6C allele yielded two products: a main product harboring exons 21, 22, and 23 (ex22+) and a minor product in which exon 22 was skipped (ex22-). cDNA derived from the construct harboring the c.2281–6G allele yielded two products: a main product in which exon 22 was skipped (ex22-) and a minor product harboring exons 21, 22, and 23 (ex22+). Interestingly, cDNA derived from the constructs harboring the c.2281–26₋₁₇ deletion, with either a C or a G at position –6, yielded only the ex22- product (Figure 5B). These results are in agreement with the in silico predictions. They suggest that some degree of alternative splicing of exon 22 may occur normally, the c.2281–6C>G polymorphic allele further weakens the intron 21 acceptor splice site and enhances the skipping of exon 22, and the c.2281–26₋₁₇ deletion leads to full skipping of exon 22.

TABLE 4. IN SILICO ANALYSIS OF *PROM1* INTRON 21 ACCEPTOR-SITE.

Position	Genotype			
c.2281–6	C	G	C	G
c.2281–26 ₋₁₇	+	+	del	del
Prediction tool	Acceptor site scores			
Splice Site Prediction by Neural Network ^a	0.90	0.49	0.47	Not scored
SplicePort ^b	0.038	–0.472	Not scored	Not scored

^aSplice Site Prediction by Neural Network threshold for acceptor splice site is 0.4^bSplicePort threshold for acceptor splice site is –10 del, deletion; +, no deletion

The PROM1 protein is 865 amino acids (aa) long. It has five transmembrane domains, with an extracellular N-terminus, a cytosolic C-terminus, and two large extracellular loops [16] (Figure 1A). Skipping of exon 22 is expected to lead to an in-frame deletion of 31 aa (p.I761-L791del). AA 761–791 are located at the second extracellular loop, adjacent to the fifth transmembrane domain (Figure 1A). Bioinformatic analysis by the [ConSurf Server](#) using 108 PROM1 orthologs predicted that the region encoded by aa 761–791 is relatively conserved and includes two structurally important residues (highly conserved and buried) and six functionally important residues (highly conserved and exposed; Figure 1B,C). In addition, [DisEMBL](#), an intrinsic protein disorder predictor, predicted that the deletion would lead to a reduced disorder at the C' end of the protein, while the [Chou and Fasman](#) secondary structure prediction server predicted loss of a turn as a result of the deletion. These predictions imply that skipping of PROM1 exon 22 would have structural and functional consequences at the protein level. These changes

appear to be tolerated if the exon 22- transcript is combined with another splice variant including exon 22 (exon 22+).

DISCUSSION

The aim of the current study was to investigate the genetic basis for CRD in a consanguineous Israeli family. Genetic analysis revealed a novel and unique intronic mutation of the *PROM1* gene. The phenotype associated with this mutation is autosomal recessive CRD, including progressive visual loss, central scotomas, photosensitivity, deficient color saturation, and slowly decreasing night vision. Judging from the medical history and the current clinical and electrophysiological data of the affected family members, we can conclude that the central scotoma slowly expands with time toward more peripheral VF regions and that night vision and VF will continue to deteriorate. A similar phenotype was described in additional patients with *PROM1* mutations (Table 1).

Of the 21 *PROM1* pathogenic mutations reported to date, six are splicing mutations. Five of these are located within canonical splice sites (Table 1). Interestingly, a deep

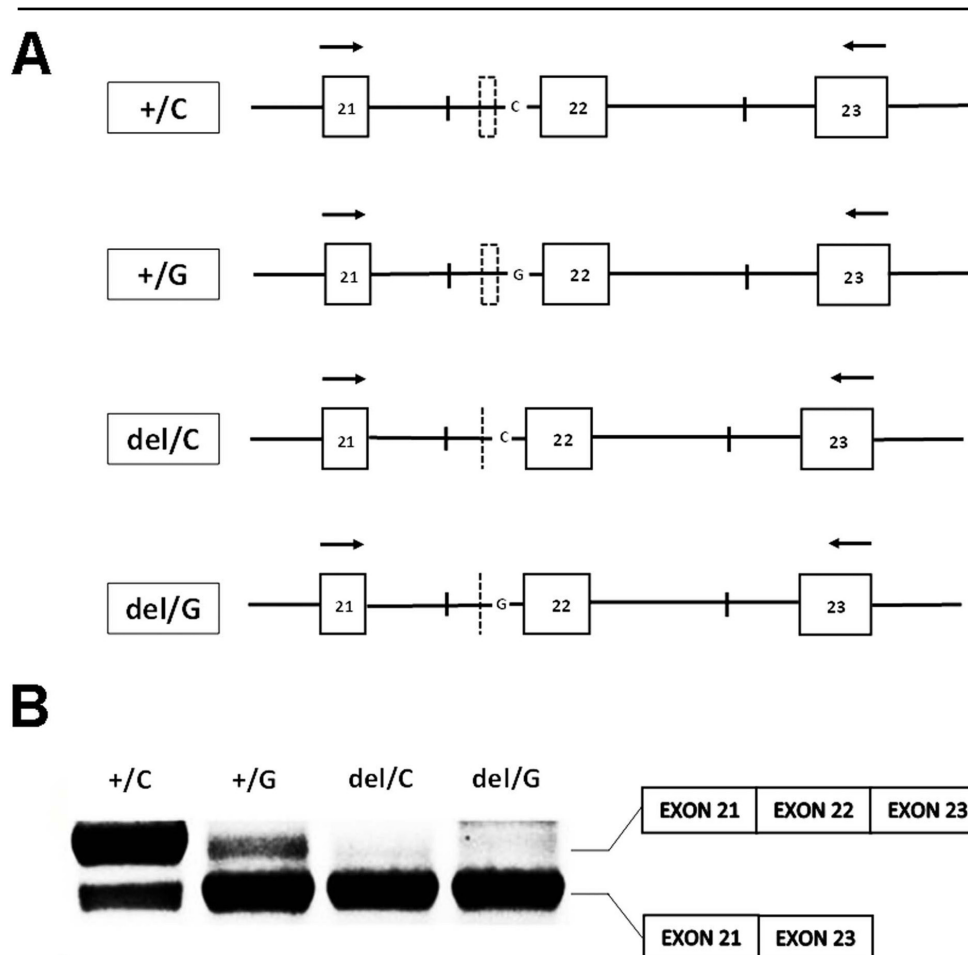


Figure 5. Minigene constructs and products obtained in the in vitro splicing assay. **A:** Shown is a schematic representation of the constructs, which include *PROM1* exons 21, 22, and 23 (represented by boxes), flanked by intronic sequences (represented by straight lines). The deletion breakpoint is indicated by a dashed line in the mutant constructs (del/C and del/G), while the deleted bases are indicated by a dashed box in the corresponding wild-type (wt) constructs (+/C and +/G). Either a C or a G is present at position -6 of intron 21. Also shown are the locations of primers used for RT-PCR analysis (indicated by arrows). **B:** Constructs were transfected into COS-7 cells, followed by RNA extraction and RT-PCR analysis. cDNA derived from wt constructs yielded two products, with and without exon 22. cDNA derived from constructs harboring the deletion yielded only the ex22- product.

intronic mutation located in *PROM1* intron 18, which leads to pseudoexon activation, was recently reported [17]. The deletion reported here is also unique, since it leaves the canonical splice site intact, and yet it affects splicing and leads to complete skipping of exon 22. This effect may result from elimination of a potential recognition site for a known splicing factor, SRSF2, which is located within the deleted sequence.

c.2281–26_–17del was linked to a known polymorphic allele, c.2281–6C>G. Based on the 1000 Genomes database, this SNP has a minor allele frequency of 17%. In our ethnically matched control group, we found an even higher allele frequency, 34%. The in silico and in vitro analyses indicated that alternative splicing of exon 22 is a normal phenomenon, which occurs to some extent in the presence of the wt allele (c.2281–6C and no deletion). The result is an in-frame deletion of 31 aa, which is predicted to yield a shorter protein variant. The presence of long and short variants may be functionally significant. The c.2281–6G allele significantly reduces the effectiveness of the intron 21 acceptor site and enhances the trend of exon 22 skipping (Table 4 and Figure 5). This effect probably results from the fact that c.2281–6C>G resides within the polypyrimidine tract and replaces a pyrimidine (C) with a purine (G). The resulting level of exon 22 skipping is surprising, given the high frequency of healthy individuals who are homozygotes for this allele. Probably in these individuals the level of *PROM1* transcripts harboring exon 22 is sufficient to maintain normal retinal function. Nevertheless, while based on our findings, complete skipping of exon 22 is not compatible with normal retinal function and leads to childhood-onset retinal degeneration, the c.2281–6G allele may be a risk factor for milder retinal phenotypes, such as age-related macular degeneration. It would be interesting to test this hypothesis by analyzing data from genome-wide association studies performed with SNP arrays that contain this common SNP. However, this is beyond the scope of the current study. In conclusion, this report expands the spectrum of pathogenic mutations of *PROM1* and further demonstrates the importance of intronic mutations.

APPENDIX 1. STR ANALYSIS OF COS-7 CELLS.

To access these data, click or select the words "Appendix 1".

ACKNOWLEDGMENTS

We are grateful to the family members for their participation in this study. This work was supported by a research grant from the Foundation Fighting Blindness (FFB; BR-GE-0214-0639-TECH) to TB, RL, HN and IP.

REFERENCES

1. Ayuso C, Millan JM. Retinitis pigmentosa and allied conditions today: a paradigm of translational research. *Genome Med* 2010; 2:34-[PMID: 20519033].
2. Hamel CP. Cone rod dystrophies. *Orphanet J Rare Dis* 2007; 2:7-[PMID: 17270046].
3. Miraglia S, Godfrey W, Yin AH, Atkins K, Warnke R, Holden JT, Bray RA, Waller EK, Buck DW. A novel five-transmembrane hematopoietic stem cell antigen: isolation, characterization, and molecular cloning. *Blood* 1997; 90:5013-21. [PMID: 9389721].
4. Yin AH, Miraglia S, Zanjani ED, Almeida-Porada G, Ogawa M, Leary AG, Olweus J, Kearney J, Buck DW. AC133, a novel marker for human hematopoietic stem and progenitor cells. *Blood* 1997; 90:5002-12. [PMID: 9389720].
5. Weigmann A, Corbeil D, Hellwig A, Huttner WB. Prominin, a novel microvilli-specific polytopic membrane protein of the apical surface of epithelial cells, is targeted to plasmalemmal protrusions of non-epithelial cells. *Proc Natl Acad Sci USA* 1997; 94:12425-30. [PMID: 9356465].
6. Yang Z, Chen Y, Lillo C, Chien J, Yu Z, Michaelides M, Klein M, Howes KA, Li Y, Kaminoh Y, Chen H, Zhao C, Chen Y, Al-Sheikh YT, Karan G, Corbeil D, Escher P, Kamaya S, Li C, Johnson S, Frederick JM, Zhao Y, Wang C, Cameron DJ, Huttner WB, Schorderet DF, Munier FL, Moore AT, Birch DG, Baehr W, Hunt DM, Williams DS, Zhang K. Mutant prominin 1 found in patients with macular degeneration disrupts photoreceptor disk morphogenesis in mice. *J Clin Invest* 2008; 118:2908-16. [PMID: 18654668].
7. Littink KW, Koenekoop RK, van den Born LI, Collin RW, Moruz L, Veltman JA, Roosing S, Zonneveld MN, Omar A, Darvish M, Lopez I, Kroes HY, van Genderen MM, Hoyng CB, Rohrschneider K, van Schooneveld MJ, Cremers FP, den Hollander AI. Homozygosity mapping in patients with cone-rod dystrophy: novel mutations and clinical characterizations. *Invest Ophthalmol Vis Sci* 2010; 51:5943-51. [PMID: 20554613].
8. Maw MA, Corbeil D, Koch J, Hellwig A, Wilson-Wheeler JC, Bridges RJ, Kumaramanickavel G, John S, Nancarrow D, Roper K, Weigmann A, Huttner WB, Denton MJ. A frameshift mutation in prominin (mouse)-like 1 causes human retinal degeneration. *Hum Mol Genet* 2000; 9:27-34. [PMID: 10587575].
9. Pras E, Abu A, Rotenstreich Y, Avni I, Reish O, Morad Y, Reznik-Wolf H, Pras E. Cone-rod dystrophy and a frameshift mutation in the *PROM1* gene. *Mol Vis* 2009; 15:1709-16. [PMID: 19718270].
10. McCulloch DL, Marmor MF, Brigell MG, Hamilton R, Holder GE, Tzekov R, Bach M. ISCEV Standard for full-field clinical electroretinography (2015 update). *Doc Ophthalmol* 2015; 130:1-12. [PMID: 25502644].
11. Grimberg J, Nawoschik S, Belluscio L, McKee R, Turck A, Eisenberg A. A simple and efficient non-organic procedure for the isolation of genomic DNA from blood. *Nucleic Acids Res* 1989; 17:8390-[PMID: 2813076].

12. Seelow D, Schuelke M, Hildebrandt F, Nurnberg P. HomozygosityMapper—an interactive approach to homozygosity mapping. *Nucleic Acids Res* 2009; 37:W593–99. [PMID: 19465395].
13. Almeida JL, Hill CR, Cole KD. Authentication of African green monkey cell lines using human short tandem repeat markers. *BMC Biotechnol* 2011; 11:102. [PMID: 22059503].
14. Fu XD, Maniatis T. The 35-kDa mammalian splicing factor SC35 mediates specific interactions between U1 and U2 small nuclear ribonucleoprotein particles at the 3' splice site. *Proc Natl Acad Sci USA* 1992; 89:1725-9. [PMID: 1531875].
15. Gallego ME, Gattoni R, Stevenin J, Marie J, Expert-Bezancon A. The SR splicing factors ASF/SF2 and SC35 have antagonistic effects on intronic enhancer-dependent splicing of the beta-tropomyosin alternative exon 6A. *EMBO J* 1997; 16:1772-84. [PMID: 9130721].
16. Corbeil D, Karbanova J, Fargeas CA, Jaszai J. Prominin-1 (CD133): Molecular and Cellular Features Across Species. *Adv Exp Med Biol* 2013; 777:3-24. [PMID: 23161072].
17. Mayer AK, Rohrschneider K, Strom TM, Glockle N, Kohl S, Wissinger B, Weisschuh N. Homozygosity mapping and whole-genome sequencing reveals a deep intronic PROM1 mutation causing cone-rod dystrophy by pseudoexon activation. *Eur J Hum Genet* 2015; •••. [PMID: 26153215].
18. Jinda W, Taylor TD, Suzuki Y, Thongnoppakhun W, Limwongse C, Lertrit P, Suriyaphol P, Trinavarat A, Atchaneyasakul LO. Whole exome sequencing in Thai patients with retinitis pigmentosa reveals novel mutations in six genes. *Invest Ophthalmol Vis Sci* 2014; 55:2259-68. [PMID: 24618324].
19. Zhao L, Wang F, Wang H, Li Y, Alexander S, Wang K, Willoughby CE, Zaneveld JE, Jiang L, Soens ZT, Earle P, Simpson D, Silvestri G, Chen R. Next-generation sequencing-based molecular diagnosis of 82 retinitis pigmentosa probands from Northern Ireland. *Hum Genet* 2015; 134:217-30. [PMID: 25472526].
20. Eisenberger T, Neuhaus C, Khan AO, Decker C, Preising MN, Friedburg C, Bieg A, Gliem M, Charbel Issa P, Holz FG, Baig SM, Hellenbroich Y, Galvez A, Platzer K, Wollnik B, Laddach N, Ghaffari SR, Rafati M, Botzenhart E, Tinschert S, Borger D, Bohring A, Schreml J, Kortge-Jung S, Schell-Apacik C, Bakur K, Al-Aama JY, Neuhann T, Herkenrath P, Nurnberg G, Nurnberg P, Davis JS, Gal A, Bergmann C, Lorenz B, Bolz HJ. Increasing the yield in targeted next-generation sequencing by implicating CNV analysis, non-coding exons and the overall variant load: the example of retinal dystrophies. *PLoS One* 2013; 8:e78496. [PMID: 24265693].
21. Zhang X, Ge X, Shi W, Huang P, Min Q, Li M, Yu X, Wu Y, Zhao G, Tong Y, Jin ZB, Qu J, Gu F. Molecular diagnosis of putative Stargardt disease by capture next generation sequencing. *PLoS One* 2014; 9:e95528. [PMID: 24763286].
22. Permanyer J, Navarro R, Friedman J, Pomares E, Castro-Navarro J, Marfany G, Swaroop A, Gonzalez-Duarte R. Autosomal recessive retinitis pigmentosa with early macular affection caused by premature truncation in PROM1. *Invest Ophthalmol Vis Sci* 2010; 51:2656-63. [PMID: 20042663].
23. Beryozkin A, Zelinger L, Bandah-Rozenfeld D, Shevach E, Harel A, Storm T, Sagi M, Eli D, Merin S, Banin E, Sharon D. Identification of mutations causing inherited retinal degenerations in the israeli and palestinian populations using homozygosity mapping. *Invest Ophthalmol Vis Sci* 2014; 55:1149-60. [PMID: 24474277].
24. Boulanger-Scemama E, El Shamieh S, Demontant V, Condroyer C, Antonio A, Michiels C, Boyard F, Saraiva JP, Letexier M, Souied E, Mohand-Said S, Sahel JA, Zeitz C, Audo I. Next-generation sequencing applied to a large French cone and cone-rod dystrophy cohort: mutation spectrum and new genotype-phenotype correlation. *Orphanet J Rare Dis* 2015; 10:85. [PMID: 26103963].
25. Khan AO, Bolz HJ. Pediatric Cone-rod Dystrophy with High Myopia and Nystagmus Suggests Recessive PROM1 Mutations. *Ophthalmic Genet* 2015; [PMID: 24547909].
26. Zhang Q, Zulfiqar F, Xiao X, Riazuddin SA, Ahmad Z, Caruso R, MacDonald I, Sieving P, Riazuddin S, Hejtmancik JF. Severe retinitis pigmentosa mapped to 4p15 and associated with a novel mutation in the PROM1 gene. *Hum Genet* 2007; 122:293-9. [PMID: 17605048].

Articles are provided courtesy of Emory University and the Zhongshan Ophthalmic Center, Sun Yat-sen University, P.R. China. The print version of this article was created on 8 December 2015. This reflects all typographical corrections and errata to the article through that date. Details of any changes may be found in the online version of the article.